Gascón Martínez, ML.; García Manrique, JA.; Lebel, F.; Ruiz, E.; Trochu, F. (2015). Numerical prediction of saturation in dual scale fibrous reinforcements during Liquid Composite Molding. Composites Part A: Applied Science and Manufacturing. 77:275-284. doi:10.1016/j.compositesa.2015.05.019.

Numerical Prediction of Saturation in Dual Scale Fibrous Reinforcements during Liquid Composite Molding

Gascón L[a,*], García JA[b], LeBel F[c], Ruiz E[c], Trochu F[c]

[a] *Depto. Matemática Aplicada, Universidad Politécnica de Valencia, Camino Vera s/n, 46022, Valencia, Spain*
[b] *Depto. Ing. Mecánica y Materiales, Universidad Politécnica de Valencia, Camino Vera s/n, 46022, Valencia, Spain*
[c] *Chair on Composites of High Performance (CCHP), Mechanical Engineering Department, Center of Research on Polymers and Composites (CREPEC), École Polytechnique de Montréal, Montréal, Canada, H3C 3A7*

Abstract

This paper presents a fractional flow model based on two-phase flow, resin and air, through a porous medium to simulate numerically Liquid Composites Molding (LCM) processes. It allows predicting the formation, transport and compression of voids in the modelling of LCM. The equations are derived by combining Darcy's law and mass conservation for each phase (resin/air). In the model, the relative permeability and capillary pressure depend on saturation. The resin is incompressible and the air slightly compressible. Introducing some simplifications, the fractional flow model consists of a saturation equation coupled with a pressure/velocity equation including the effects of air solubility and compressibility. The introduction of air compressibility in the pressure equation allows for the numerical prediction of the experimental behaviour at low constant resin injection flow rate. A good agreement was obtained between the numerical prediction of saturation in a glass fiber reinforcement and the experimental observations during the filling of a test mold by Resin Transfer Moulding (RTM).

Keywords: B. Porosity; C. Computational Modelling; E. Resin Transfer Moulding (RTM)

1. Introduction

Understanding the formation of voids in LCM is necessary for proper manufacturing of composite structural parts. Many studies exist on void formation in LCM. A comprehensive review of these methods in [1] and [2] confirms the interest of understanding void creation mechanisms and transport in order to develop

*Corresponding author. Tel: +34 963879662
Email address: llgascon@mat.upv.es (Gascón L)

new optimisation strategies. Despite continual progress in the last decades, still many unresolved issues and limitations exist in current numerical approaches.

The resin flow in a partially saturated region can be modeled as a two-phase flow (resin and air) through a porous medium. The numerical modeling and analysis of two-phase flows in porous media has arisen interest for several years and different approaches have been developed. However few studies were carried out in LCM with the multiphase approach. Pillai and Advani [3] were the first to propose a two-phase flow model in LCM based on the Buckley-Leverett formulation. Later, Chui et al. [4] implemented the Buckley-Leverett model numerically, using a front-tracking scheme, to predict the distribution of voids in RTM. They considered the relative permeability to depend on saturation and pressure. More recently, Nordlund and Michaud [5] have also applied a numerical multiphase flow model derived from soil mechanics to LCM processes. It is based on the Richard's equation, combined with van Genuchten expressions for the saturation and relative permeability. In this case, an optimal combination of the parameters of van Genuchten's equations has been calculated from the experimental and numerical data using a curve fit optimization by the Response Surface Method.

The equations of two-phase flow are derived from Darcy's law and mass conservation for each phase (resin/air). The property of the fluid fills up the volume and capillary pressure is given as a function of saturation to close the system of equations. In this case, relative permeability depends on the degree of saturation of the fibrous reinforcement and describes how each phase flows with respect to the other. Hence, the choice of a constitutive relation between relative permeability and saturation represents a key issue in LCM processes to describe the fluid flow.

In order to analyze the formation of voids during reinforcement impregnation, a one-dimensional solution based on two-phase flow through a porous medium has been proposed by Gascon et al. [6]. This model is based on a fractional formulation and leads to a coupled system of a nonlinear advection-diffusion equation for saturation and an elliptic equation for pressure and velocity. In [6] permeability was assumed to be a quadratic function of saturation and the continuity equation that governs the pressure distribution includes a source term depending on saturation. Not only can the choice of relative permeability have a significant

impact on the predicted saturation, but the quality of the approximation is also affected by the numerical method used to solve the saturation equation. In [6] the elliptic pressure equation was approximated by finite elements and a modified flux limiter technique [7] applied to solve the saturation equation.

In order to test and evaluate the ability of the proposed model, the numerical results of saturation were compared to experimental injections carried out in a glass RTM mold under controlled manufacturing conditions [8]. The experimentally observed saturation for different constant injection flow rates were compared to numerical simulations. The validation of the mathematical model and of the numerical technique was performed for a moderate constant resin injection rate of 0.1 ml/s [6, 9]. Numerical results in agreement with experiments were obtained with the new fractional flow model with a quadratic power law to model the relative permeability and a modified flux limiter technique to simulate the evolution of saturation in the mold. However, the model did not reproduce the filling behaviour of the mold at lower constant injection flow rates when the effect of capillary forces becomes significant. As observed in Fig. 1 experimental results show that the resin saturation increases at the beginning and then decreases in time at the break points. This indicates the necessity to model a new behaviour connected with void formation and transport in the numerical simulation of LCM processes. As described in detail in the sequel, it appears that air compressibility plays an important role in this case.

It is well known that multiphase flows in porous media exhibit hysteresis [10]. The relative permeability and capillary pressure have long been recognized in multiphase processes to depend not only on saturation, but also on the direction of saturation changes. This hysteretic behaviour is typically modeled by modifying the model of relative permeability as a function of saturation and using different expressions of capillary pressure, depending on the imbibition or drainage stages during the filling process (see Fig. 2).

The objective of this study is propose a new model to simulate LCM processes taking into account void formation, and air compression and transport. This requires an hyperbolic conservation law for the saturation equation coupled with an appropriate pressure equation. The numerical model presented here introduces two parameters, related to air dissolution and compressibility, in the sink source of the pressure equation, from which velocity is computed. The model also includes capillary effects in the saturation

equation. By adjusting these parameters, it is possible to simulate the formation and transport of voids in LCM and model the behaviour observed in Fig. 1 at low constant resin injection flow rate, namely 0.025 ml/s here, as an effect of air compressibility.

The paper is organized as follows. Firstly, a short description of the saturation experiments is presented. After a brief introduction on the general conservation equations and the constitutive laws for two-phase flows (resin and air), the new fractional flow formulation with pressure and resin saturation as primary unknowns is introduced in Section 3. The predictions of the new model are validated in Section 4 by comparison with the results of injection experiments at constant flow rate. Concluding remarks are presented in Section 5. Finally, a short derivation of the equations is included in the Appendix.

2. Experimental study

In order to test and evaluate the new two-phase flow model proposed in this investigation to predict the evolution of saturation, numerical results of saturation are compared with the experiments reported in [8], where unidirectional RTM injections were carried out at room temperature and atmospheric pressure in a rectangular mold with transparent glass cover. The geometry considered is a rectangular mold cavity of 360 mm in length, 105 mm in width and of thickness 3.175 mm. In order to analyze saturation, the flow domain was divided in a grid of 21 by 5 Representative Elementary Volumes (REV) along the length and width, respectively. Saturation was evaluated in each REV and an average value was calculated along the width of the piece. Each REV has a dimension of 15 mm by 15 mm. Right after the inlet port and just before the vent, two narrow bands of 22.5 mm long by 105 mm wide were not analyzed.

Saturation was evaluated by 2D tomographic reconstruction using a visible light transmission (VLT) method. This experimental technique is based on fundamental relationships of optics. It allows a better understanding of the mechanisms of void formation and transport in dual scale fibrous reinforcements [8, 11]. The 2D tomographic reconstruction method by visible light transmission is a non-intrusive technique allowing the dynamic monitoring of saturation in transparent fibrous reinforcements such as the E-glass reinforcement used in the current investigation. This monitoring technique is based on two fundamentals of optics, namely

the Beer-Lambert's law and the Fresnel's law, and it takes advantage of the refractive index matching between the E-glass filament and the translucent thermoset resin in order to increase the visual contrast of entrapped voids. In this regard, these latter voids appear as zones of lower transmitted light intensity.

The Beer-Lambert's law is relating the transmission of light to the properties of the medium through which the light is travelling. As a matter of fact, this optical law states a logarithmic dependency between the light transmission through a medium and the product of the distance the light travels through this given medium with the absorption coefficient of the corresponding medium material. On the other hand, the Fresnel's law gives the light transmission factor at a diopter interface, assuming normal incidence. From these two optical laws, a transfer function can be established between the transmitted intensity of visible light I_x at a given location of the translucent reinforcement to its corresponding local saturation level S_r^e as follows:

$$S_r^e = \frac{\ln\left(\left[\frac{I_{\text{unsat}} - \left(I_{\text{unsat}}^{\text{ref}} / I_{\text{dry}}^{\text{ref}}\right) \cdot I_{\text{dry}}}{I_{\text{sat}} - \left(I_{\text{sat}}^{\text{ref}} / I_{\text{dry}}^{\text{ref}}\right) \cdot I_{\text{dry}}}\right] \cdot \left[\left(\frac{I_{\text{sat}} - B}{I_{\text{dry}} - B}\right) - \frac{I_{\text{sat}}^{\text{ref}}}{I_{\text{dry}}^{\text{ref}}}\right] + \frac{I_{\text{unsat}}^{\text{ref}}}{I_{\text{dry}}^{\text{ref}}}\right)}{\ln\left(\frac{I_{\text{sat}} - B}{I_{\text{dry}} - B}\right)} \tag{1}$$

where I_{dry}, I_{unsat} and I_{sat} are respectively the transmitted light intensities through the reinforcement for the completely dry state, the unsaturated states and the fully saturated state. On the other hand, $I_{\text{dry}}^{\text{ref}}$, $I_{\text{unsat}}^{\text{ref}}$, $I_{\text{sat}}^{\text{ref}}$ and B are correction factors to account for light source noise and background noise based on direct measurements of light source intensity as well as background intensity (i.e. the intensity when no light is transmitted).

These experimental measurements of transmitted light intensity are carried out using a digital camera with a wide-angle lens set under the transparent RTM mold, a white light source set over the mold, a light diffuser and monochromatic filters inserted between the light source and the mold. In this specific configuration, a transparent cavity frame gives direct visual access to the light source for the digital camera as shown in Fig. 3. Details on this experimental investigation on saturation in fibrous reinforcements can be found in [8].

In this study, saturation results are taken for two experimental injections carried out at different constant flow rates, at 0.025 ml/s and 0.1 ml/s, which correspond to capillary numbers of 0.00225 and 0.009

repectively. The intrinsec permeability K, the resin viscosity μ and porosity ϕ have been set to 7.9×10^{-10} m^2, 0.4788 Pa.s and 0.614, respectively.

Fig. 1 shows the experimental saturation measured at different times during mold filling. Each curve represents the evolution of saturation in a different strip of 5 REVs along the width of the grid. As seen in Fig. 4, the shape of each saturation curve in time is divided in two distinct areas by a break point. The slope and position of the break points will be used for the numerical validation of the proposed saturation models. When resin saturation increases from one break point to the next one on the right the process can be considered to be in a secondary imbibition stage. On the contrary, when resin saturation decreases after the break points, a secondary drainage process rather takes place in terms of saturation.

3. Numerical modeling

The resin flow in a partially saturated region can be modeled as a two-phase flow (resin and air) through a porous medium. Equations describing immiscible two-phase isothermal flows in a fixed mold cavity and within an undeformable and immobile reinforcement are given by the mass balance equation and Darcy's law for each of the phases, respectively:

$$\phi \frac{\partial}{\partial t} \left(\rho_\alpha S_\alpha \right) + \nabla \cdot \left(\rho_\alpha \mathbf{q}_\alpha \right) = 0 \quad , \quad \alpha = r,\ a \tag{2}$$

$$\mathbf{q}_\alpha = -\lambda_\alpha \left(S_\alpha \right) \nabla p_\alpha \quad , \quad \alpha = r,\ a \tag{3}$$

where r denotes the wetting phase (resin) and a the non wetting phase (air). The porous medium is characterized by its porosity ϕ and intrinsic permeability K; the phase velocity $\mathbf{q}_\alpha$ is defined by Darcy's law and ρ_α, S_α , μ_α and p_α are, respectively, the density, saturation, viscosity and pressure of the α phase. The other porous medium properties are the relative permeability and capillary pressure, which are given as a function of saturation. The mobility of the phase α is defined as

$$\lambda_\alpha \left(S_\alpha \right) = \frac{K k_{r,\alpha} \left(S_\alpha \right)}{\mu_\alpha} \tag{4}$$

where $k_{r,\alpha}(S_\alpha)$ is the relative permeability of the porous medium for phase α. Additionally, the system satisfies the following volume constraint:

$$S_r + S_a = 1 \tag{5}$$

which assures that the two-phases fill all the available pore space. Hence in the sequel, we note $S_r = S$ and $S_a = 1 - S$. The capillary pressure defined by

$$p_c(S) = p_a - p_r \tag{6}$$

depends on saturation. Following the standard definitions of the literature, the capillary pressure on the pore scale is defined as the difference between the non wetting (air) and wetting (resin) phase pressures. However on the macroscale level, the capillary pressure has been commonly considered to be a function of the wetting phase saturation only. Finally, to complete the system, constitutive relationships between saturation, relative permeability and capillary pressure are needed. In this work, following the results of [6], a quadratic power law has been chosen to express the relative permeability dependency upon resin saturation as follows:

$$k_{r,r}(S) = S^2 \quad , \quad k_{r,a}(S) = (1-S)^2 \tag{7}$$

Furthermore, the resin is incompressible (ρ_r is constant) and the air density is given by the ideal gas law. Hence, we set

$$\widetilde{c}_a = \frac{1}{\rho_a}\frac{\partial \rho_a}{\partial p_a} \tag{8}$$

where $\widetilde{c}_a$ is the air compressibility coefficient, given by a positive constant. In this work, the viscosity of the air and of the resin is supposed constant and gravity is neglected.

The mass conservation equations for each phase form a system of equations which can be coupled in different ways. Summing Eqns. 2 and regrouping the terms, a fractional flow formulation is obtained with pressure and resin saturation as primary unknowns [12]. Hence, the total mass conservation writes as follows (see Appendix)

$$\nabla \cdot \mathbf{q}_t = -\phi \frac{\partial}{\partial t}\left(\rho_r S + \rho_a(p_a)(1-S)\right) \tag{9}$$

where the total flow is defined as

$$\mathbf{q}_t = \rho_r \mathbf{q}_r + \rho_a(p_a)\mathbf{q}_a \tag{10}$$

The resin phase equation for saturation takes the following form

$$\phi\rho_r \frac{\partial S}{\partial t} + \nabla \cdot (\mathbf{q}_t \ f(S)) = -\nabla \cdot (D_c(S)\nabla S) \tag{11}$$

where the resin fractional flow function $f(S)$ and the diffusive coefficient $D_c(S)$ depend on resin saturation as follows:

$$f(S) = \frac{\rho_r \lambda_r(S)}{\rho_r \lambda_r(S) + \rho_a(p_a)\lambda_a(S)} \tag{12}$$

$$D_c(S) = f(S)\rho_a(p_a)\lambda_a(S)\frac{\partial p_c}{\partial S} \tag{13}$$

Equations (9), (10) and (11) form a system of nonlinear partial differential equations, strongly coupled through the dependence on saturation in the pressure equation and through the dependence of the total flow appearing in the saturation equation.

As described in Appendix, the proposed model introduces simplifications which allow reproducing the saturation behaviour observed in the experimental results and weakens the coupling between Eqns. (9), (10) and (11). The resulting equations written in a fractional flow formulation lead to a coupled system which consists of a nonlinear advection-diffusion for saturation and an elliptic equation for pressure. In this formulation, the pressure p and the resin saturation S are chosen as primary variables. Hence, the numerical simulation of the filling process involves the following operations at each time step:

1. The saturation distribution from the previous step (or initial data) is used to compute the saturation dependent coefficients in the following pressure equation

$$\nabla \cdot \left(\frac{K}{\mu_r}\nabla p\right) = \phi\,(1-\chi)\,\frac{\partial S}{\partial t} - \phi c_a\,(1-S)\,\chi \tag{14}$$

Two parameters have been included in the sink source of the pressure equation: χ which controls air dissolution and c_a which takes into account air compressibility. Note that, in general, these functions depend on pressure although excellent numerical results have been obtained with constant terms.

2. Calculate the velocity field from equation

$$\mathbf{q} = -\left(M^{-1}\right) \frac{K k_{r,r}\left(\widehat{S}\right)}{\mu_r} \nabla p \tag{15}$$

where

$$\widehat{S} = S + (M\chi)^{1/2}(1 - S) \tag{16}$$

with

$$M = \frac{\rho_a}{\rho_r} \frac{\mu_r}{\mu_a} \tag{17}$$

denoting the inverse of the endpoint mobility ratio.

3. Update saturation using a numerical method based on a modified flux limiter technique to solve the following equation

$$\phi \frac{\partial S}{\partial t} + \nabla \cdot (\mathbf{q}\ f(S)) = -\nabla \cdot (D \nabla S) \tag{18}$$

where $f(S)$ represents the resin fractional flow

$$f(S) = \frac{S^2}{S^2 + M(1 - S)^2} \tag{19}$$

The diffusive term in Eqn. (18) includes capillary effects as follows:

$$D(S) = \frac{K}{\mu_r} M (1 - S)^2 f(S) \frac{\partial p_c}{\partial S} \tag{20}$$

Standard boundary conditions are used with no pressure gradient in the normal direction to the mold walls, specified flow rate on the inflow boundary and zero pressure in the empty part of the mold.

The pressure equation was solved by a standard Galerkin finite element method on the same mesh as in the fluid volume technique used to find an updated approximation of saturation at each time step. The domain is divided in N uniformly spaced elements with cells $\left[x_{j-1/2,}, x_{j+1/2}\right]$ of width h. At each time step, the pressure at the nodes $x_{j+1/2}$ is calculated by standard finite elements. After pressure is determined, the velocity at the centre of the finite elements is computed by differentiating the nodal fluid pressure in Eqn. (15). Then, using the velocity field derived from the solution of the pressure equation, saturation is calculated explicitly. The saturation S is assumed constant in each element and is determined by a flux

limiter technique. Hence the following discretization of the saturation equation is proposed

$$S_j^{n+1} = S_j^n - \frac{\Delta t}{h}\left(\widehat{F}_{j+1/2}^{+} - \widehat{F}_{j+1/2}^{-}\right) - (\Delta t)\, C_j^n \tag{21}$$

where Δt denotes the uniform time step; $\widehat{F}_{j+1/2}^{\pm}$ and C_j^n are the numerical approximations on the time step t_n of the flux function $\mathbf{F}$ and the diffusive term C, which are defined by

$$\mathbf{F} = \frac{\mathbf{q}}{\phi} f(S) \quad , \quad C = \frac{1}{\phi}\nabla \cdot (D_c(S)\nabla S) \tag{22}$$

The accuracy of the discretization will be mainly related to the computation of the fluxes $\mathbf{F}$ at the interfaces. Hence, a classical discretization for the diffusive term C can be considered while the numerical fluxes are given by

$$\widehat{F}_{j+1/2}^{\pm} = \widehat{F}_{j+1/2}^{L\pm} + L\left(r_{j+1/2}^{\pm}\right)\left[\widehat{F}_{j+1/2}^{H} - \widehat{F}_{j+1/2}^{L\pm}\right] \tag{23}$$

where $\widehat{F}_{j+1/2}^{L\pm}$ are upwind first order numerical fluxes defined as

$$\widehat{F}_{j+1/2}^{L+} = \frac{1}{2}\left\{F_j + F_{j+1} - \text{sign}\left(\mathbf{q}\frac{\partial f}{\partial S}\right)_{j+1}(F_{j+1} - F_j)\right\} \tag{24}$$

$$\widehat{F}_{j+1/2}^{L-} = \frac{1}{2}\left\{F_j + F_{j+1} - \text{sign}\left(\mathbf{q}\frac{\partial f}{\partial S}\right)_{j}(F_{j+1} - F_j)\right\} \tag{25}$$

and $\widehat{F}_{j+1/2}^{H}$ denotes a second order numerical flux given by

$$\widehat{F}_{j+1/2}^{H} = \frac{1}{2}\left\{F_j + F_{j+1} - \frac{\Delta t}{h\phi}\left(\mathbf{q}\frac{\partial f}{\partial S}\right)_{j+1/2}(F_{j+1} - F_j)\right\} \tag{26}$$

This numerical approximation is based on the flux limiter strategy described in [7] to calculate the void fraction in LCM. The idea is to develop a numerical algorithm with the smoothing capability of a lower order scheme when necessary and the accuracy of a higher order scheme when possible (see [7, 13] for more details). Hence, Eqn. (23) is defined as a hybrid scheme that uses high order fluxes in smooth regions of the solution with a limitation on the numerical fluxes to avoid numerical oscillations in the vicinity of the discontinuous values. The flux limiter function L in Eqn. (23) is a smoothness indicator that prevents non monotone behaviour at the expense of a certain loss of accuracy. In this work, the superbee limiter has been used

$$L(r) = \max\{0, \min(2r, 1), \min(r, 2)\} \tag{27}$$

and the coefficients $r^{\pm}$ in Eqn. (23) have been defined as a function of the ratio of consecutive gradients of saturation following a similar reasoning as in [7].

4. Results and discussion

In order to validate the mathematical model, the predicted saturation was compared with injection experiments at constant flow rates of 0.1 ml/s and 0.025 ml/s, which correspond to capillary numbers of 0.009 and 0.00225 respectively.

Experimental and numerical saturation profiles for the injection at constant flow rate of 0.1 ml/s are displayed in Fig. 5 as a function of position for different times. Numerical results in Fig. 5 have been obtained using the model proposed in the above section (see Eqs. (14), (15) and (18)), for the following parameter values:

$$M^{-1} = 1 \ , \ \chi = 0.32 \ , \ c_a = 0 \tag{28}$$

As observed in Fig. 5, numerical results obtained at a constant flow rate of 0.1 ml/s match correctly and show the same behaviour as experimental observations. The new fractional flow model calculates saturation, pressure and velocity with a quadratic power law model for relative permeability and a flux limiter technique to simulate the saturation equation. The numerical results exhibit an excellent agreement with experimental solutions for this test, when capillary effects are ignored in the saturation equation. In this case, air compressibility is not an important factor. However the parameter χ, which controls air dissolution, has been adjusted in order to simulate the transport of voids.

A comparison between experimental and numerical saturation curves as a function of time is shown in Fig. 6 at three different positions along the length of the test mold (REV3, REV10 and REV16) for the injection at constant flow rate of 0.025 ml/s. Numerical results represented by straight lines have been obtained with the same numerical model as the one used to compute the results of Fig. 5. This means that air compressibility and capillary effects have been ignored to compute the numerical solution of Fig. 6. In order to reproduce the correct position of saturation curves in time the endpoint mobility ratio, defined as the ratio between the maximum velocity of the displacing fluid (resin) and the maximum velocity of the

displaced fluid (air) by the density ratio, has been taken with values greater than unity. In this simulation, the following parameters have been used:

$$M^{-1} = 1.2 \ , \ \chi = 0.32 \ , \ c_a = 0 \tag{29}$$

The position of the break points in the numerical simulation in Fig. 6 always decreases in time, indicating only void formation and transport are numerically simulated, which corresponds to a secondary drainage process at the flow front. Numerical results show the necessity to incorporate in the model the physical phenomena of air compressibility and capillary effects at low flow front velocity. As matter of fact, in this case capillary forces play an important role. Fig. 7 shows numerical results when the fractional flow function $f(S)$ in the saturation equation has been modified to include capillary effects following a typical imbibition capillary pressure function for a two-phase flow [14], given by

$$p_c(S) = p_i \ (1 - S)^{-1/2} \tag{30}$$

Numerical results of Fig. 7 have been computed using the following parameters:

$$M^{-1} = 1.2 \ , \ \chi = 0.32 \ , \ c_a = 0 \ , \ p_i = 200 \tag{31}$$

As seen in Fig. 7, numerical results can reproduce saturation when the break point is maximum. However the model cannot predict the change of behaviour observed in experiments. A comparison between Figs. 6 and 7 illustrates that the different evolutions of saturation can be numerically simulated. However, in order to take into account the change between these two different behaviours, air compressibility must also be included in the model.

The numerical results of Fig. 8 show how air compressibility changes the predicted saturation. The figure shows the experimental saturation as a function of time for three REVs considered and the comparison with the numerical solution for the injection at constant flow rate of 0.025 ml/s simulated using the fractional flow model with the following parameters

$$M^{-1} = 1.2 \ , \ \chi = 1 \tag{32}$$

Here, the air compressibility coefficient c_a has been adjusted by

$$c_a = \begin{cases} 7 \times 10^{-4} & , \quad p_1 < p < p_2 \\ 0 & , \quad \text{else} \end{cases} \tag{33}$$

where p_1 and p_2 are critical pressures between which the voids are compressed. In the case of low injection flow rates, mesoscopic voids are created at the flow front during mold filling. Experiments show that initially the saturation at the break points tends to decrease at the flow front during the first iterations (before 500 s approximately) because of the formation of voids. As the flow front moves, some voids remain entrapped in the fiber bed, while others move with the resin flow [4]. Once the voids are created at the flow front, the resin pressure rises with time as the injection proceeds. Hence, some entrapped air bubbles decrease in sizes due to the progressive increase in pressure. Therefore there is a critical pressure, named p_1 in Eqn. (33), above which voids are compressed and decrease in size until another critical pressure p_2 is reached for which voids can be mobilized again. Note that the introduction of a critical pressure for void mobilization has been also considered in [15]. After this second pressure level is reached, saturation at the break points decreases until the end of mold filling. Hence, air compression has been included in the model for the two critical pressure levels $p_1 = 2800\ Pa$ and $p_2 = 6800\ Pa$ to compute the numerical results in Figs. 8, 9 and 10.

Experimental and numerical resin saturation profiles for the injection at constant flow rate of 0.025 ml/s are given as a function of position for different values of time in Fig. 9. A good agreement was found between the numerical and experimental solutions. As seen from experimental results, saturation data exhibit a non monotone oscillatory profile, developing overshoots before the break points are reached. This could be explained by a faster resin velocity as a consequence of a new distribution of pore sizes after the air has been compressed. Therefore endpoint mobility values greater than unity are needed in order to reproduce the correct positions of the saturation curves like in other two-phase flow problems.

Numerical results of Fig. 10 reproduce the experimental observations of saturation in Fig. 1. The numerical results of Figs. 8, 9 and 10 show that the new fractional model, including air dissolution, air compresibility and capillary effects in the saturation equation, represents correctly the critical experimental

phenomena. From the experiments carried out in [8] and as already observed by several researchers [1, 16] when looking at the experimental saturation curves in time for the two different injection flow rates considered, it is clear that the impregnation velocity plays a key role on air entrapment at the flow front. However, pressure is also important since it governs the compression and dissolution of air bubbles in the resin flow. The numerical and experimental results obtained at lower injection flow rates are consistent with these observations.

Finally, in order to validate the proposed model on another geometry, the 1D numerical solution of saturation in the divergence nozzle of Fig. **??** has been computed (dimensions are expressed in mm). Numerical results of saturation as a function of time at six different positions along the divergent nozzle are illustrated in Fig. 12. Saturation curves correspond to the injection at constant flow rate of 0.1 ml/s, at the left, and of 0.025 ml/s, at the right. The tests have been simulated using the same conditions and the same parameters as in the previously considered cases. The numerical saturation distribution calculated with the fractional two-phase flow at four filling times of 250 s, 600 s, 1200 s and 1800 s for the injection at constant flow rate of 0.1 ml/s is plotted in Fig. 13. The conduct was divided in 24 elements where the area of each element represents its volume. The next step would be the extension of the model to 2D or 3D complex problems.

5. Conclusion

In the current work a new two-phase flow model (resin/air) was developed and implemented to study the formation, compression and transport of air bubbles in LCM processes. The model is based on a fractional flow formulation with pressure and resin saturation as primary unknowns and two coupled equations: a nonlinear advection-diffusion equation for saturation (transport) and a new elliptic equation for pressure and velocity (flow). The equations can be efficiently solved using the finite element method to approximate the pressure equation and a flux limiter technique to solve the saturation equation. In this formulation, the relative permeability and capillary pressure are assumed to depend on saturation. Two parameters have been introduced to incorporate air dissolution and compressibility in the model.

The model and the numerical scheme have been validated by comparing simulation results with experimental data. Although some simplifications have been carried out from the original mass conservation and Darcy equations describing the two-phase flow process in porous media, the agreement between experimental and numerical predictions for two different RTM injection flow rates demonstrates that the model can successfully predict saturation in LCM. Furthermore, the numerical procedure incorporates the important physical features of void formation and transport with the effect resulting from air compressibility that comes into play in RTM injections at lower injection flow rates. This formulation opens up new opportunities to improve LCM flow simulations and optimize injection molds.

Acknowledgments

The authors acknowledge financial support of the Spanish Government (Project DPI2010-20333).

Appendix A. Governing equations

The basic equations describing two-phase flow in a porous medium are given by the mass balance equation and Darcy's law for each of the fluid phases, resin (r) and air (a) in this case. In addition, we also have the property that the two phases fill the available pore space and the capillary pressure law given by Eqn. (6). We start from Eqn. (2), which describes mass conservation for the resin and air phases, respectively

$$\nabla \cdot (\rho_r \mathbf{q}_r) = -\phi \frac{\partial}{\partial t} (\rho_r S) \tag{A.1}$$

$$\nabla \cdot (\rho_a(p_a) \mathbf{q}_a) = -\phi \frac{\partial}{\partial t} (\rho_a(p_a)(1-S)) \tag{A.2}$$

The total mass conservation is obtained by adding the two members of the above equations

$$\nabla \cdot \mathbf{q}_t = -\phi \frac{\partial}{\partial t} (\rho_r S + \rho_a(1-S)) \tag{A.3}$$

where the total flow is defined as

$$\mathbf{q}_t = \rho_r \mathbf{q}_r + \rho_a \mathbf{q}_a \tag{A.4}$$

Since resin and air velocities are governed by Darcy's law from Eqn. (3),

$$\mathbf{q}_r = -\lambda_r(S)\,\nabla p_r \tag{A.5}$$

$$\mathbf{q}_a = -\lambda_a(S)\,\nabla p_a \tag{A.6}$$

in view of the capillary pressure law given by Eqn. (6) the total flow can be rewritten as

$$\mathbf{q}_t = -\left(\rho_r\lambda_r(S) + \rho_a\lambda_a(S)\right)\nabla p_r - \rho_a\lambda_a(S)\,\nabla p_c \tag{A.7}$$

Denoting the resin fractional flow function $f(S)$ by

$$f(S) = \frac{\rho_r\lambda_r(S)}{\rho_r\lambda_r(S) + \rho_a\lambda_a(S)} \tag{A.8}$$

and the diffusive coefficient $D_c(S)$ due to capillary effects by

$$D_c(S) = f(S)\rho_a\lambda_a(S)\frac{\partial p_c}{\partial S} \tag{A.9}$$

the following expression is derived when Eqn. (A.7) is multiplied by $f(S)$

$$f(S)\mathbf{q}_t = \rho_r\mathbf{q}_r - D_c(S)\nabla S \tag{A.10}$$

which, combined with mass conservation for the resin (Eqn. (A.1)), leads to the saturation equation

$$\phi\rho_r\frac{\partial S}{\partial t} + \nabla\cdot\left(\mathbf{q}_t\ f(S)\right) = -\nabla\cdot\left(D_c(S)\nabla S\right) \tag{A.11}$$

The resulting system for pressure and saturation is given by Eqns. (A.3), (A.4) and (A.11) and it can be summarized as

$$\nabla\cdot\mathbf{q}_t = -\phi\frac{\partial}{\partial t}\left(\rho_r S + \rho_a(1-S)\right) \tag{A.12}$$

$$\mathbf{q}_t = \rho_r\mathbf{q}_r + \rho_a\mathbf{q}_a \tag{A.13}$$

$$\phi\rho_r\frac{\partial S}{\partial t} + \nabla\cdot\left(\mathbf{q}_t\ f(S)\right) = -\nabla\cdot\left(D_c(S)\nabla S\right) \tag{A.14}$$

After dividing all equations by ρ_r (constant) and carrying out differentiation with respect to time on the right hand side of the pressure equation, the system takes the following form

$$\nabla \cdot \widetilde{\mathbf{q}}_t = -\phi \left(1 - \frac{\rho_a}{\rho_r}\right) \frac{\partial S}{\partial t} - \phi(1-S)\frac{\rho_a}{\rho_r}\widetilde{c}_a \frac{\partial p_a}{\partial t} \tag{A.15}$$

$$\widetilde{\mathbf{q}}_t = \mathbf{q}_r + \frac{\rho_a}{\rho_r}\mathbf{q}_a \tag{A.16}$$

$$\phi\frac{\partial S}{\partial t} + \nabla \cdot (\widetilde{\mathbf{q}}_t \; f(S)) = -\nabla \cdot \left(\widetilde{D}_c(S)\nabla S\right) \tag{A.17}$$

where

$$f(S) = \frac{\lambda_r(S)}{\lambda_r(S) + \frac{\rho_a}{\rho_r}\lambda_a(S)} \tag{A.18}$$

$$\widetilde{D}_c(S) = f(S)\frac{\rho_a}{\rho_r}\lambda_a(S)\frac{\partial p_c}{\partial S} \tag{A.19}$$

and

$$\widetilde{c}_a = \frac{1}{\rho_a}\frac{\partial \rho_a}{\partial p_a} \tag{A.20}$$

denotes the air compressibility.

Our goal now is to introduce some simplifications in the equations so as to weaken the coupling between saturation and pressure/velocity in our model of LCM processes. For that purpose, three constant parameters χ , M and c_a have been introduced in the equations to capture the physical behaviour of the original strongly coupled system. The parameter χ has been defined as the maximum void fraction in the mold during the injection. Another important parameter in determining the effectiveness of two-phase flow displacement is the endpoint mobility ratio defined as the ratio between the maximum velocity of the displacing fluid (resin) and the maximum velocity of the displaced fluid (air) by the density ratio. The endpoint mobility ratio is defined as the inverse of

$$M = \frac{\rho_a}{\rho_r}\frac{\mu_r}{\mu_a} \tag{A.21}$$

The value of M is very important to decide the correct position of the discontinuity in the resin saturation at the flow front. Finally, in order to incorporate air compressibility effects included in the second term on the right hand side of Eqn. (A.15) a third parameter c_a is introduced.

A detailed explanation of the equations ignoring air compressibility has been presented in [6]. For this purpose, we have assumed that all air bubbles are transported in the flow and move at the same velocity as the resin. The above assumptions result in an expression of the elliptic pressure equation similar to that of the resin phase where the relative permeability used to calculate the velocity has been replaced by $k_{r,r}(\widehat{S})$ with

$$\widehat{S} = S + (M\chi)^{1/2}(1-S) \tag{A.22}$$

The fractional flow formulation to model LCM process proposed in [6] can be summarized as

$$\nabla \cdot \left(\frac{K}{\mu_r} \nabla p \right) = \phi (1-\chi) \frac{\partial S}{\partial t} \tag{A.23}$$

$$\mathbf{q} = -\frac{K k_{r,r}(\widehat{S})}{\mu_r} \nabla p \ , \tag{A.24}$$

$$\widehat{S} = S + (M\chi)^{1/2}(1-S) \tag{A.25}$$

$$\phi \frac{\partial S}{\partial t} + \nabla \cdot (\mathbf{q}\ f(S)) = -\nabla \cdot (D(S) \nabla S) \tag{A.26}$$

where $f(S)$ represents the resin fractional flow

$$f(S) = \frac{S^2}{S^2 + M(1-S)^2} \tag{A.27}$$

and the diffusive term including capillary effects is given by

$$D(S) = \frac{K}{\mu_r} M (1-S)^2 f(S) \frac{\partial p_c}{\partial S} \tag{A.28}$$

The definition of $f(S)$ and $D(S)$ is based on quadratic expressions of the relative permeability as a function of saturation.

Numerical predictions of saturation based on this fractional two-phase flow formulation agreed well with experiments for intermediate flow rates [6], as in the case of the injection at constant flow rate of 0.1 ml/s. However, new hypotheses are needed for slower and larger injection flow rates. Firstly, in order to allow the resin and air to flow at different speeds, the total velocity has been multiplied by the endpoint mobility ratio (M^{-1}). Secondly, the right hand side of the pressure equation includes now a second term taking into account air compressibility. Hence, the new fractional flow formulation for pressure and saturation to model

LCM process can be summarized as follows:

$$\nabla \cdot \left(\frac{K}{\mu_r} \nabla p \right) = \phi \left(1 - \chi\right) \frac{\partial S}{\partial t} - \phi c_a \left(1 - S\right) \chi \tag{A.29}$$

$$\mathbf{q} = -\left(M^{-1}\right) \frac{K k_{r,r}(\widehat{S})}{\mu_r} \nabla p \ , \tag{A.30}$$

$$\widehat{S} = S + \left(M\chi\right)^{1/2} \left(1 - S\right) \tag{A.31}$$

$$\phi \frac{\partial S}{\partial t} + \nabla \cdot \left(\mathbf{q}\ f(S)\right) = -\nabla \cdot \left(D(S) \nabla S\right) \tag{A.32}$$

Note that the introduction of the air compressibility in the pressure equation allows modelling the behaviour observed in the experimental injections at low constant injection flow rates. However, this remains a difficult numerical problem because the original pressure equation changes from elliptic to parabolic, when air compressibility depends on pressure.

References

[1] Park CH, Lee W. Modeling void formation and unsaturated flow in liquid composite molding processes: a survey and review. J Reinf Plast Compos 2011; 30 (11): 957-977.

[2] Pillai KM. Modeling the Unsaturated Flow in Liquid Composite Molding Processes: A Review and Some Thoughts. J Compos Mater 2004; 38 (23): 2097-2118.

[3] Pillai KM, Advani SG. Modeling of Void Migration in resin Transfer Molding Process. In: Proceedings of the 1996 ASME International Mechanical Engineering Congress and Exhibition. Atlanta GA, 1996.

[4] Chui, WK, Glimm J, Tangerman FM, Jardine AP, Madsen JS, Donnellan TM, Leek R. Process Modeling in Resin Transfer Molding as a Method to Enhance Product Quality. SIAM Review 1997; 39(4): 714-727.

[5] Nordlund M, Michaud V. Dynamic saturation curve measurement for resin flow in glass fibre reinforcement. Compos Part A: Appl Sci Manufact 2012; 43: 333-343.

[6] Gascón Ll, García JA, Ruiz E, Lebel F, Trochu F. A two phase flow model to predict saturation in Liquid Composite Molding 2015, Int J Mater Form 2015. DOI: 10.1007/s12289-015-1225-z.

[7] García JA, Gascón Ll, Chinesta F. A fixed mesh numerical method for modelling the flow in liquid composites moulding processes using a volume of fluid technique. Comp Methods Appl Mech Engrg 2003; 192 (7-8): 877-893.

[8] Lebel, F. Contrôle de la fabrication des composites par injection sur renforts. PhD thesis École Polytechnique de Montréal, 2012.

[9] García JA, Gascón Ll, Ruiz E, Lebel F, Trochu F. Simulation and experimental validation of the saturation in LCM

processes. In Procedings of the 11th International Conference on Flow Processes in Composite Materials. Auckland, NZ, 2012. p.127-135.

[10] Plohr BD, Marchesin P, Bedrikovetsky, Krause P. Modeling hysteresis in porous media flow via relaxation. Computational Geosciences 2001; 5: 225-256.

[11] Lebel F, Fanaei A, Ruiz E, Trochu F. Experimental Characterization by Fluorescence of Capillary Flows in the Fiber Tows of Engineering Fabrics. Open Journal of Inorganic Non-Metallic Materials 2012; 2(3): 25-45.

[12] Amaziane B, Jurak M, Zgaljić Keko A. Modeling and numerical simulations of immiscible compressible two-phase flow in porous media by the concept of global pressure. Transp Porous Media 2010; 84: 133-152.

[13] García JA, Gascón Ll, Chinesta F. A flux limiter strategy for solving the saturation equation in RTM process simulation. Compos Part A: Appl Sci Manufact 2010; 41: 78-82.

[14] Brooks RH, Corey AT. Hydraulic properties of porous media. Colorado State University Hydrology Papers 1964; 1-37.

[15] Gourichon B, Binetruy C, Krawczak P. A new numerical procedure to predict dynamic void content in liquid composite molding. Compos Part A: Appl Sci Manufact 2006; 37(11): 1961-1969.

[16] Ruiz E, Achim V, Soukane S, Trochu F, Bréard F. Optimization of injection flow rate to minimize micro/macro-voids formation in resin transfer molded composites. Compos Sci Technol 2006; 66(3-4): 475-486.

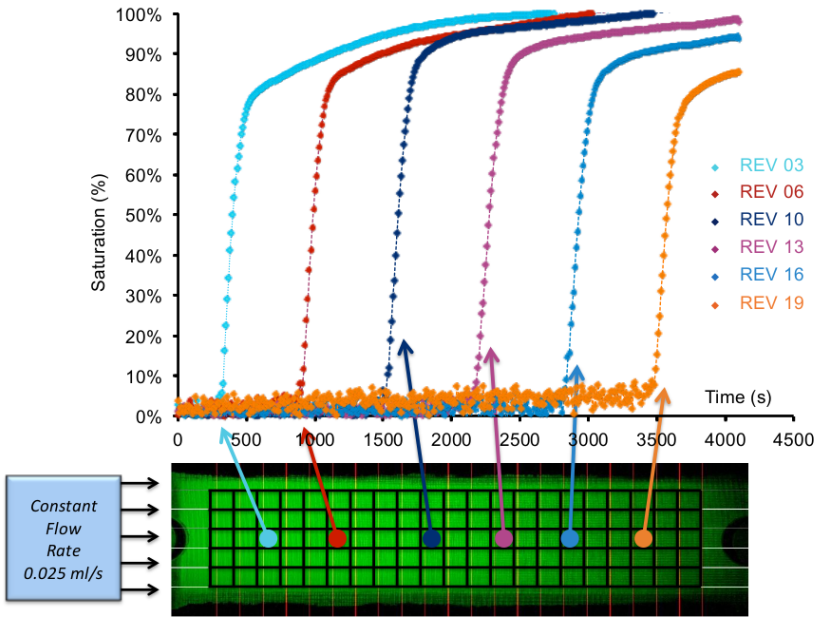

Figure 1: Schematic representation of experimental saturation at different times during mold filling for the injection at constant flow rate of 0,025 ml/s.

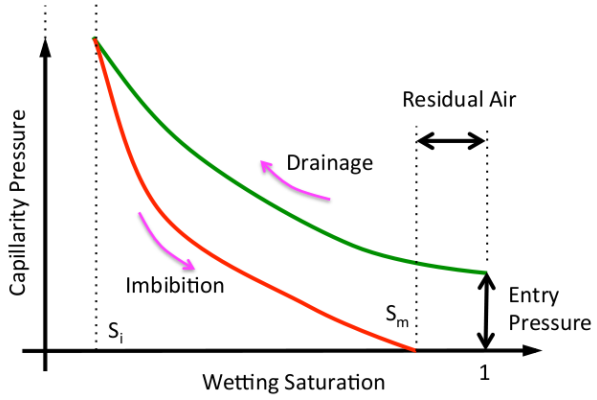

Figure 2: Typical drainage and imbibition capillary pressure curves in two-phase flow.

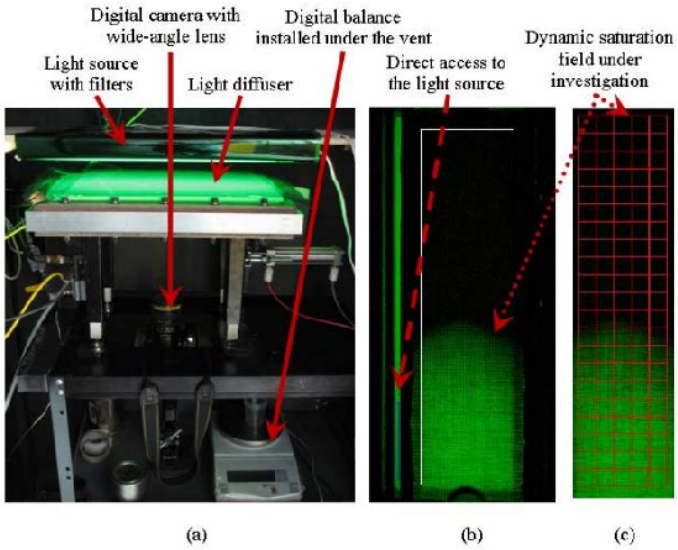

Figure 3: The complete optical setup: (a) RTM mold with transparent glass covers, a digital camera and a filtered light source; (b) typical image acquisition of the dynamic saturation of the glass fibrous reinforcement; (c) calculations of dynamic saturation on a REV based grid (21 REV by 5 REV).

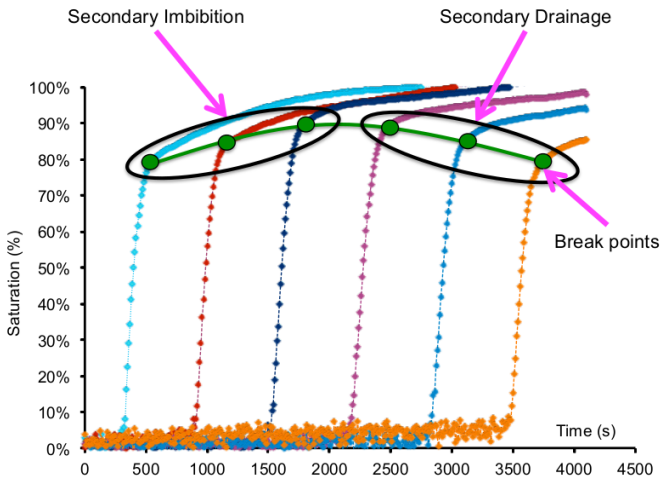

Figure 4: Experimental saturation at different times during mold filling.

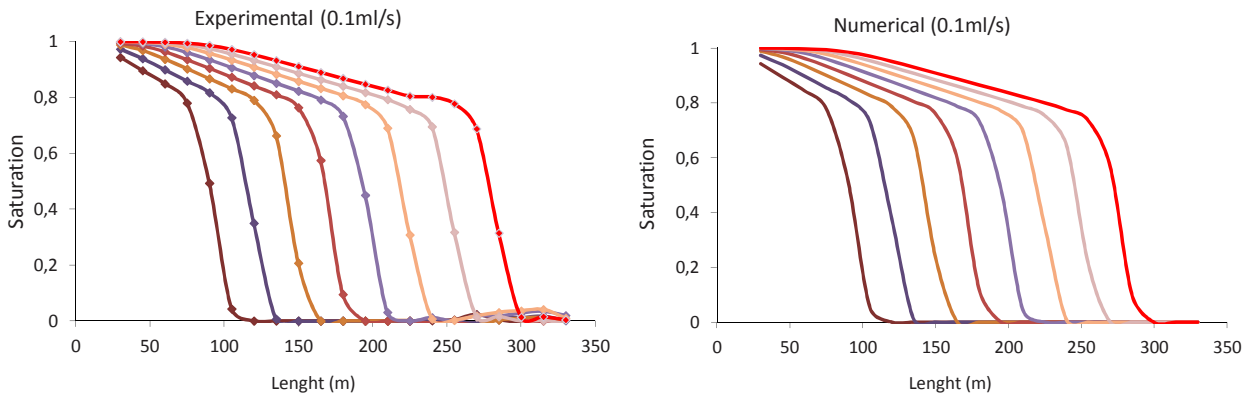

Figure 5: Experimental and numerical resin saturation as a function of position at different times for the injection at constant flow rate of 0.1 ml/s.

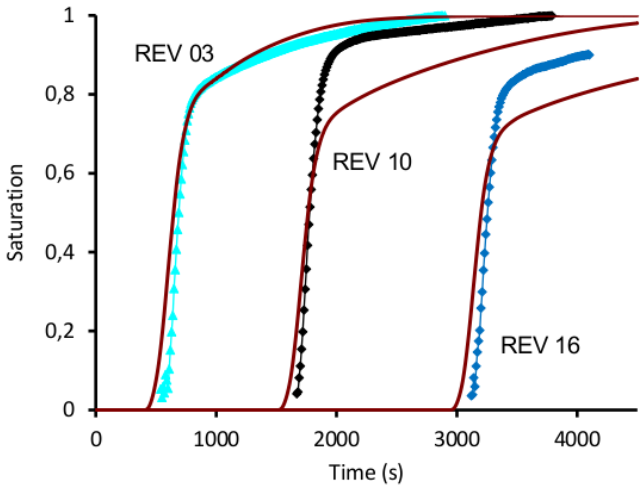

Figure 6: Experimental and numerical curves of saturation as a function of time for three REV for the injection at constant flow rate of 0.025 ml/s. Numerical results are represented by straight lines. Air compressibility and capillary effects have not been taken into account in the saturation equation.

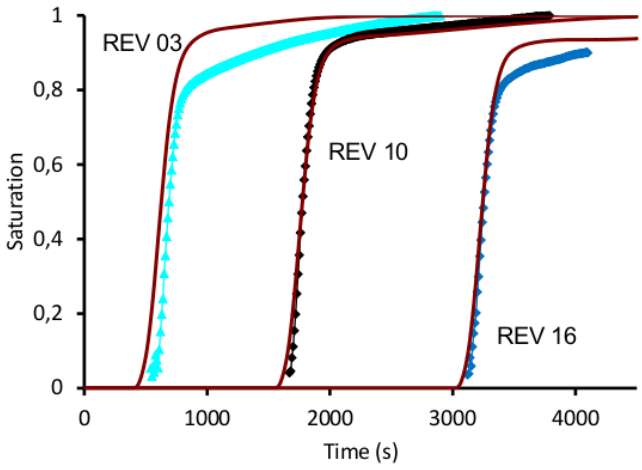

Figure 7: Experimental and numerical curves of saturation as a function of time for three REV for the injection at constant flow rate of 0.025 ml/s. Numerical results, represented by straight lines, have been obtained without air compressibility, but by considering the capillary pressure given by Eqn. (30) in the saturation equation.

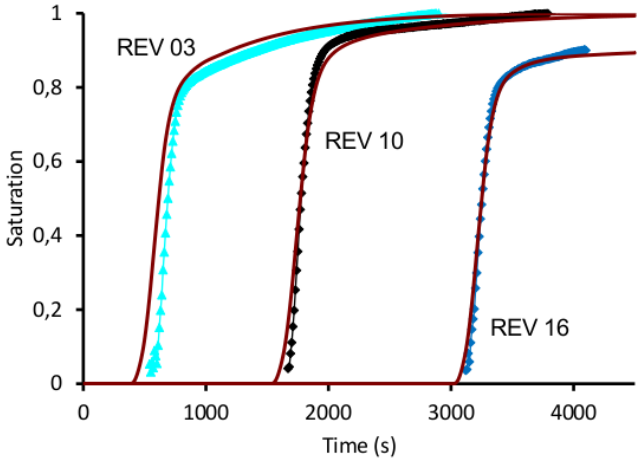

Figure 8: Experimental and numerical curves of saturation as a function of time for three REV for the injection at constant flow rate of 0.025 ml/s. Numerical results, represented by straight lines, include air compressibility as described by Eqn. (33) and the capillary pressure given by Eqn. (30) in the saturation equation.

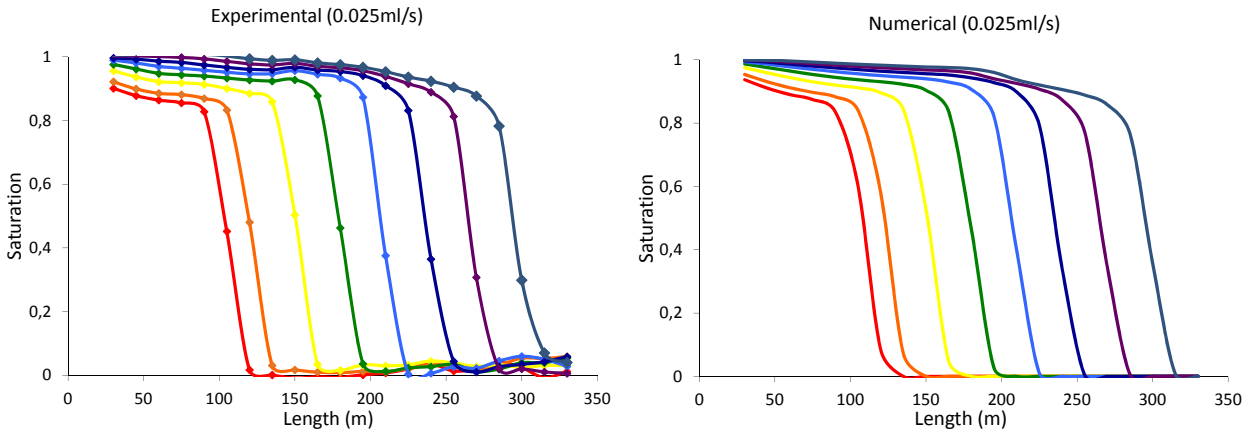

Figure 9: Experimental and numerical saturation as a function of position at different times for the injection at constant flow rate of 0.025 ml/s. Numerical simulation incorporates air compressibility effects, described by Eqn. (33), and the capillary pressure given by Eqn. (30) in the saturation equation.

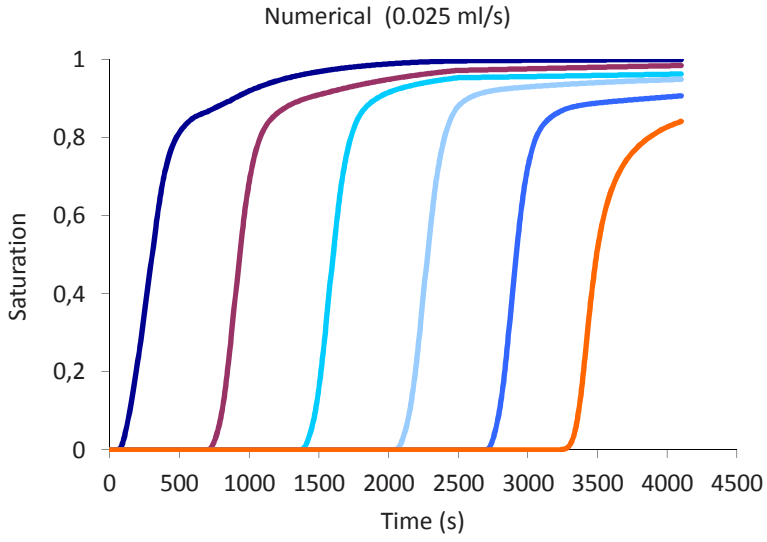

Figure 10: Numerical curves of saturation as a function of time for the injection at constant flow rate of 0.025 ml/s. Numerical results including air compressibility effects, described by Eqn. (33), and the capillary pressure given by Eqn. (30) in the saturation equation, reproduce perfectly the experimental data of Fig. 1.

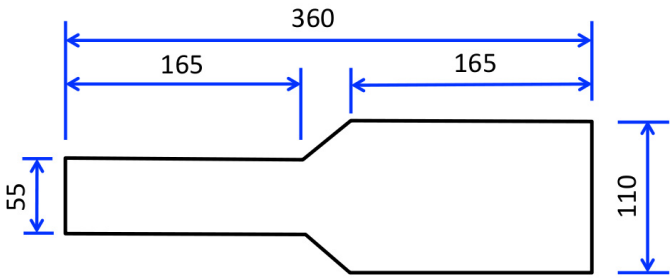

Figure 11: Divergent nozzle dimensions (mm).

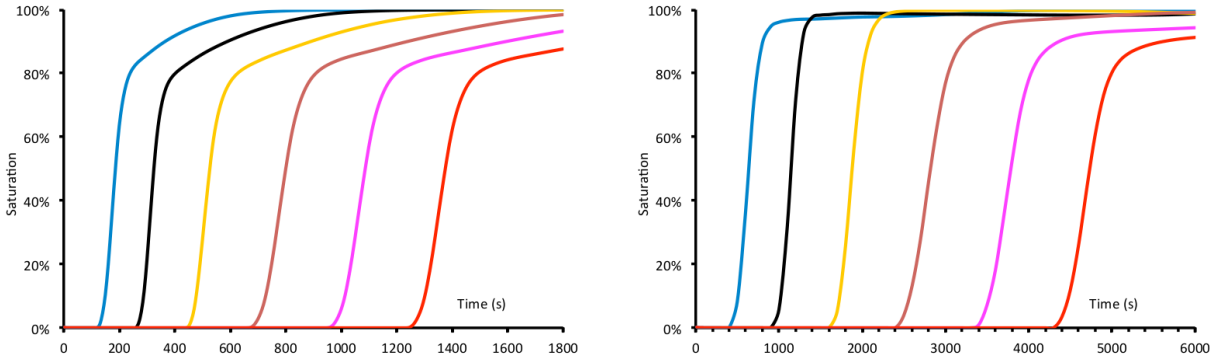

Figure 12: Numerical curves of saturation as a function of time at six different positions along the divergent nozzle of Fig. **??** injecting at constant flow rate of 0.1 ml/s, at the left, and injecting at constant flow rate of 0.025 ml/s, at the right.

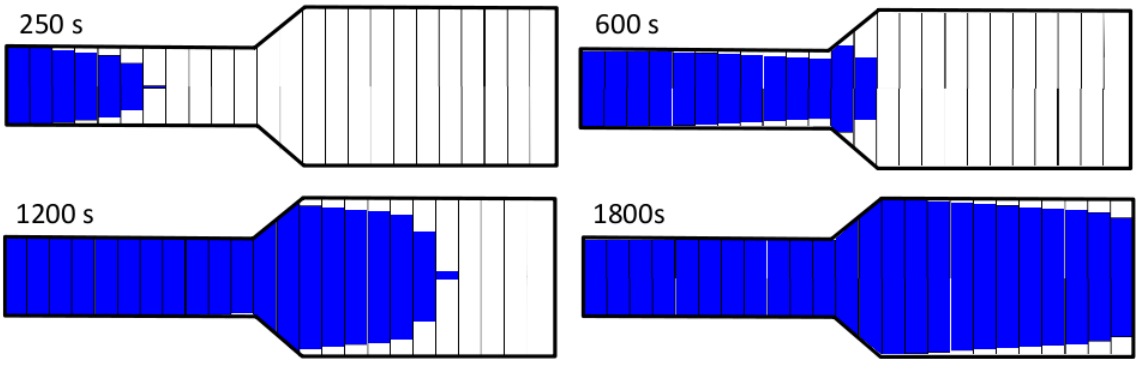

Figure 13: Numerical saturation at four filling times of 250 s, 600 s, 1200 s and 1800 s for the injection at constant flow rate of 0.1 ml/s.

Nomenclature

α	subscript for phase (r resin, a air)
$\mathbf{q}_\alpha$	velocity of the phase α
$\mathbf{q}_t$	total flow
$\mathbf{q}$	total velocity approximation
p_α	pressure of the phase α
p	pressure approximation
$p_c(S)$	capillary pressure
ρ_α	density of the phase α
μ_α	viscosity of the phase α
ϕ	porosity
S_α	saturation of the phase α ($S_r = S$)
K	intrinsic permeability
$k_{r,\alpha}(S)$	relative permeability of the phase α
$\lambda_\alpha(S)$	mobility of the phase α
χ	parameter that controls the void fraction
M	inverse of the endpoint mobility ratio
$\widetilde{c}_a$	air compressibility coefficient
c_a	parameter that controls the air compressibility
$f(S)$	fractional flow
$\mathbf{F}(S)$	flux function in saturation equation
$C(S)$	diffusive fuction in saturation equation
$D(S),\ D_c(S)$	diffusive coefficients in saturation equation
$\widehat{F}^{L\pm}_{j+\frac{1}{2}}\ ,\ \widehat{F}^{H}_{j+\frac{1}{2}}$	first and second order numerical fluxes
$L(r^{\pm}_{j+\frac{1}{2}})$	limiter function to avoid oscillations
$p_1,\ p_2$	critical pressures between which air is compressible
p_i	Leverett coefficient in capillary pressure